International Journal of ISSI, Vol. 13 (2016), No. 1, pp. 39-45

Microstructural Evolution of Roll Bonded Al-Clad Stainless Steel Sheets at Elevated Temperatures

H. R. Akramifard [1] , H. Mirzadeh [2*], M. Habibi Parsa [3]

College of Engineering, School of Metallurgy & Materials Engineering, University of Tehran, Tehran 6619-14155, Iran

Abstract

The cold roll bonding of Al on AISI 304L stainless steel was carried out to fabricate the Al/304L/Al clad sheet composites. The maximum bond strength of 20 N/mm was acquired just by 38% reduction, for which the tearing of the aluminum sheet occurred during the peeling test. The microstructural evolution during subsequent post-annealing heat treatment was systematically studied based on the impurity diffusion coefficients, microhardness measurements, X-ray diffraction (XRD) patterns, scanning electron microscopy (SEM) images and energy dispersive X-ray analysis (EDS) spectra to pave the way for successful applications of these composite sheets. An intermediate layer composed of intermetallics of Al and Fe was found to form on the aluminum side of the roll bonded sheets, showing that this layer was formed by the diffusion of elements from the 304L sheet to the aluminum sheet due to the faster diffusion of Fe in Al. Moreover, the calculated diffusion distances were in a good agreement with the results obtained from the line scan EDS analysis and the microhardness profile. It was also found that the presence of the strain-induced martensite in the 304L sheet did not exert any effect on the intermediate layer.

Keywords: Cold roll cladding; Heat treatment; Peel test; Diffusion; Intermetallic compounds.

1. Introduction

Clad sheet materials have become increasingly popular as a result of their unique properties [1-3]. The cold roll bonding (CRB) is the most common process to develop clad sheet composites due to its efficiency and cost-competitiveness [4].

Stainless steel alloys have relatively high strength and can be further hardened by mechanical working due to strain-induced martensitic transformation [5], while the aluminum alloys have relatively high thermal/electrical conductivity and lower density. Generally, both classes of materials have good corrosion resistance and high ductility. Therefore, their combination can be used to produce clad sheets with unique properties. These clad sheets are supposed to exhibit a combination of high strength, good corrosion resistance, high thermal and electrical conductivity, cost-competitiveness and high specific weight, which can find applications in automotive industry, cookware, electronics, aerospace, ship building, cryogenic and chemical applications [2, 6, 7].

After the roll bonding process, the as-rolled clad sheets are usually heat treated to enhance the bond strength, in which the selection of appropriate annealing temperature and time is very important [1, 4, 6, 8, 9]. It has been reported that the bond strength of clad sheets made of different materials is increased during post heat treatment due to the interdiffusion of elements at the interface, reaching a maximum value, and decreased due to the formation of an intermediate layer deleterious for bond quality [8, 10, 11]. For instance, Movahedi et al [8] reported that the optimum bond strength could be obtained by post heat treatment at 450 °C for 90 min in AA1100/St-12 roll bonded sheets, and the formation of the intermediate layer was observed at 500 °C. Jin and Hong [1] observed the formation of interfacial compounds at temperatures above 500 °C between Al and stainless steel interface. The formation of Fe_2Al_5 and $FeAl_3$ intermetallic compounds at the interface of Fe/Al clad sheets was detected by Wang et al [12], leading to effectively deterioration of the bond quality. Lee et al [3] have reported that no intermetallic was found at the interface of stainless steel/Al after heat treatment at 400 °C for 30 min.

Formation of an intermediate layer during post-annealing is related to impurity diffusion of roll bonded clad sheets elements at high enough temperatures and times. There are several methods for the calculation

* *Corresponding author*
Tell: +98 21 611 14127
Email: hmirzadeh@ut.ac.ir
Address: College of Engineering, School of Metallurgy & Materials Engineering, University of Tehran, Tehran, Iran.
P.O. Box: 6619-14155
1. M.Sc.
2. Assistant Professor
3. Professor

of impurity diffusion coefficients [13, 14], such as DCEP-MA (diffusion couple method with electron probe microanalysis), DCM (diffusion couple method), IIMLS (ion implantation with microtome and lathe sectioning), IIMS (ion implantation with microtome sectioning), LS (lathe sectioning), MBS (Mössbauer spectroscopy), MS (microtome sectioning), RC (residual activity method), RM (resistometric method) and XRE (X-ray emission microanalysis). This implies that different pre-exponential factors (D_0) and activation energies (Q) and therefore, different diffusion coefficients based on the Arrhenius equation of the type $D = D_0 \exp(Q/RT)$ are available for the diffusion of each element [15].

In the current work, the roll bonding strength [16,18] and the development of the intermediate layer during post annealing heat treatment of Al-clad stainless steel sheets were studied based on the impurity diffusion coefficients, microhardness measurements, X-ray diffraction (XRD) patterns, scanning electron microscopy (SEM) images and energy dispersive X-ray analysis (EDS) spectra. It should be noted that the roll bonding mechanism, the mechanical properties, and the relation between roll bonding strength and tensile test results of Al-clad stainless steel sheets have been studied before [17, 18] and the present work mainly deals with the formation of intermetallic compounds based on different approaches, in which the effect of the presence of martensite can be unraveled.

2. Experimental Materials and Procedure

The materials used in the present work were the commercially pure aluminum (AA1050 alloy) and AISI 304L stainless steel (See Table 1). Degreasing and wire brushing of four contacting surfaces of the Al/304L/Al sheets were carried out by a circumferential stainless steel brush (operating at a rotation speed of 2600 rpm) to remove any contaminant layer present on the surface of the contacting sheets and to work-harden the surfaces. As shown in Fig. 1, the three-layer Al/304L/Al clad sheets were fabricated by roll bonding at room temperature under the unlubricated condition with different reductions in thickness to investigate the strength of the bond by peeling test according to ASTM-D1876-01 standard. The peeling tests were carried out using a universal tensile testing machine. The schematic of the process with its details is also shown in Fig. 1.

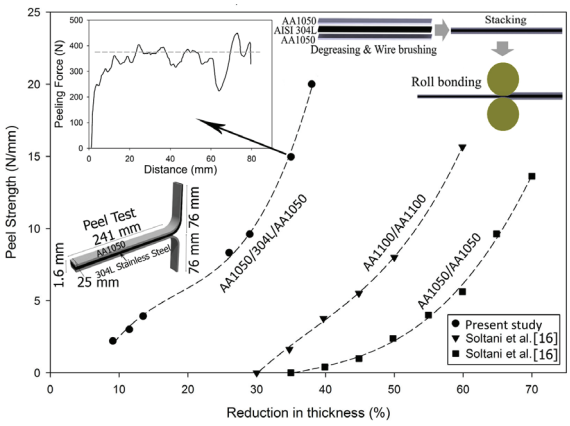

Fig. 1. Peel strength vs. reduction in thickness, an example of peeling graphs, and the schematic representation of the three-layer cladding process and peel test.

The initial thickness of AA1050 and 304L was 1 and 1.2 mm, respectively, and the final thickness of AA1050 and 304L layers after reduction in the thickness of 50% (M_{Room} specimen) was 0.45 and 0.7 mm, respectively. The 304L counterpart in M_{Room} specimen had a martensitic-austenitic structure. Therefore, the roll bonding process was also carried out at 100 °C with the reduction in the thickness of 50% to maintain the austenitic structure (A_{Room} specimen). M_{Room} and A_{Room} specimens were heat treated at 600 °C for 1h to study the interface interactions and investigate the effect of martensite on phase formation during post-annealing. It should be noted that the selection of 600 °C for 1h as the annealing condition was based on the preliminary experiments to find a good condition for the formation of the thick enough intermediate layer between Al and steel sheets.

Field emission scanning electron microscopy (Using a Zeiss FE-SEM), X-ray diffraction (using a Philips PW-3710 diffractometer with Cu Kα radiation), optical microscopy and Vickers microhardness measurements (using a load of 50 g) were used to investigate the intermediate layer.

Table 1. Chemical compositions of the sheets used in the present research.

AA1050									
Element	Al	Si	Fe	Cu	Mn	Mg	V	Ti	Zn
wt.%	99.54	0.139	0.244	0.006	0.010	0.001	0.008	0.009	0.003
AISI 304L Stainless Steel									
Element	C	Mn	Ni	Cr	Mo	Si	P	S	Fe
wt.%	0.023	1.43	8.05	18.47	0.089	0.476	0.019	0.0002	Balance

3. Results

3.1. Peel test results

Fig. 1 shows the variation of average peel strength with reduction in thickness at room temperature for AA1050304/L/AA1050 sheets (present study) and two other roll bonded Al sheets (taken from the literature). The average peel strengths (σ_{Peel}) were determined using the equation σ_{Peel} = F/W, where F is the average load of the fluctuating portion of the peeling force diagram (as shown in Fig. 1 for the reduction in the thickness of 35%) and W is the bond width. The threshold reduction required to make a suitable bond for the AA1050304/L/AA1050, AA1050/AA1050 [16], and AA1100/AA1100 [16] sheets is <10%, 35%, and 30%, respectively. Similarly, a very low threshold reduction of 10% has also been reported for the CRB of AA1050 on the medium carbon steel (ST37) three-layered sheets [11]. Moreover, the maximum bond strength of ~ 20 N/mm was determined for the AA1050304/L/AA1050 clad sheet just by 38% reduction in the present work, for which the tearing of the Al sheet occurred during the peeling test. This implied that the strength of the bond had reached the strength of Al. This is obvious advantage over the traditional CRBed AA1050/AA1050 sheets, in which the bond strength reaches ~ 14 N/mm after a heavy reduction of ~ 70% [16]. Therefore, the good cold weldability as a result of the strong affinity of Al and steel [17, 18] is obvious and a sound bond can be readily obtained, which is a key advantage for future applications of Al-clad stainless steel sheets.

3.2. Microstructural investigations

Based on the literature [1, 3, 8, 11], the temperature and time of post heat treatment should be high enough to insure complete interdiffusion between elements of sheet metal layers and the formation of the intermediate layer with some investigable thickness. Therefore, the annealing temperature of 600 °C and the annealing time of 1h were chosen in the current work. The roll-bonded specimens subjected to post heat treatment at 600 °C for 1h with initial austenitic and martensitic-austenitic microstructures were denoted as A_{600} and M_{600}, respectively.

Fig. 2 shows the FE-SEM micrographs of M_{Room} and M_{600} specimens near the Al/304L interface region. It could be seen that the roll bonding interface was not perfect and in some areas, the good bond was missing. This could be ascribed to the mechanism of roll bonding, [17] i.e., extrusion of Al through the surface cracks and settlement inside the 304L surface valleys due to the strong affinity between Al and Fe. These imperfections might adversely affect the mechanical properties of the roll bonded sheets. Moreover, the formation of an intermediate layer between Al and 304L stainless steel could be seen easily at the interface of M_{600} specimen. This phenomenon could be ascribed to the impurity diffusion at 600 °C between the elements present in Al and 304L stainless steel. Development of a longitudinal crack was observed between the intermediate layer and Al boundary due to the difference in the thermal expansion coefficients: 17.3 K^{-1} for the 304L stainless steel and 25.0 K^{-1} for Al [1, 19, 20]. As shown in Fig. 2b, the propagation of the cracks resulted in the development of a very poor bond which was easily debonded even by hands. It should be noted that the intermediate layer sat on the 304L side after debonding, which was also confirmed by XRD patterns taken from both sides of the debonded interface.

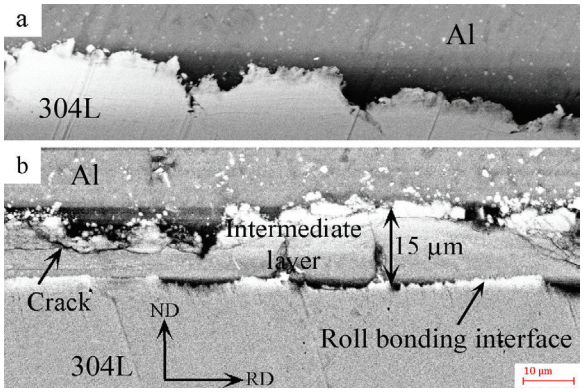

Fig. 2. Fe-SEM images around the roll bonded interface for (a) M_{Room} (b) M_{600}.

3.3. Elemental analysis of the intermediate layer

Fig. 3a shows EDS point analysis taken from the intermediate layer, revealing that elements such as Al, Fe, C, Cr, Ni, Si, and Mn were present in the intermediate layer. The high amounts of Al and Fe were logical because they were the main elements of the contacting sheets. The unexpected high amount of detected C in the intermediate layer, while it was qualitative, might be ascribed to its small size, more mobility, and the availability of more empty interstitial positions [21]. The availability of Cr, Ni, Si, and Mn was consistent with the chemical compositions shown in Table 1. It should be noted that the detection of the elements present in the intermetallic compounds by EDS point [10, 12] and line [3, 6, 8, 19] scan techniques can be a usual procedure although phase analysis techniques are required for the confirmation of the results.

Fig. 3b shows the EDS line scans of various elements from the Al side toward the 304L side of the M600 specimen. It could be easily seen that the intermediate layer was composed of Al, Fe, C, Cr, Ni, Si, and Mn, which was consistent with Fig. 3a. The sudden change in the EDS's counts per second (CPS) values for different elements could be attributed to their incorporation in the diffusion or formation

of the intermediate layer. Based on these sudden changes, the thickness of the intermediate layer plus the diffused distance could be estimated as 40 µm. However, the optical and SEM micrographs revealed that the thickness of the intermediate layer in the M_{600} specimen was about 9-17 µm. Therefore, it could be concluded that the diffused distance in the sheets (except the intermediate layer) was roughly 20 µm.

It should be noted that the type of intermetallic compounds can also be determined by EDS analysis if the chemical compositions of the roll bonded sheets are not complex. For instance, the identification of Fe_2Al_5 and $FeAl_3$ intermetallic compounds at the interface of Fe/Al clad sheets has been reported using EDS point analysis, based on the simple chemical compositions of the roll bonded sheets [12]. However, this was not the case in the present study due to the presence of several alloying elements in the roll bonded sheets. Therefore, the XRD analysis was considered for phase identification.

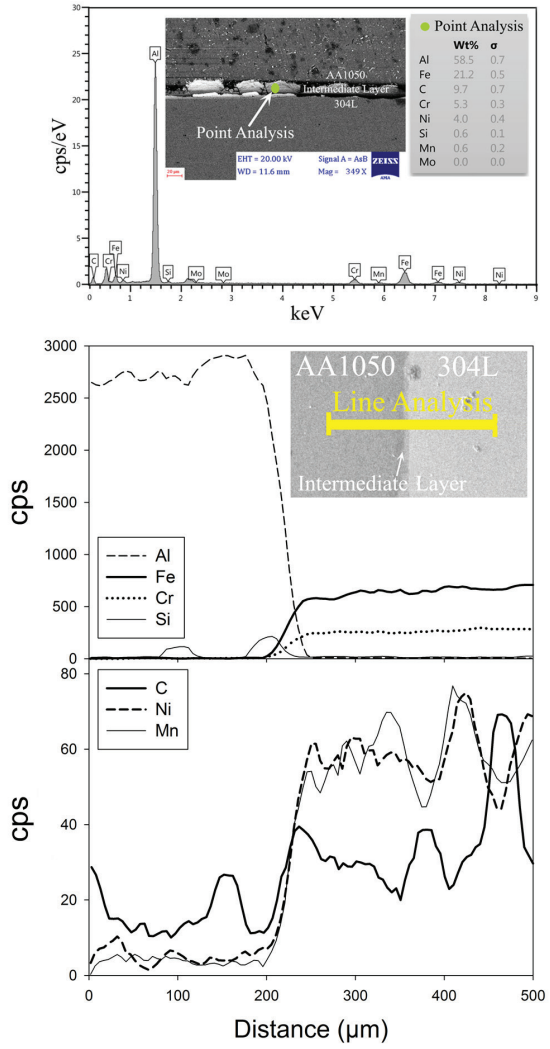

Fig. 3. EDS analysis: (a) Point scan analysis taken from the intermediate layer of M_{600} specimen and (b) Line scans analysis taken form the Al to 304L of M_{600} specimen.

3.4. Phase analysis of the intermediate layer

Fig. 4 shows the XRD patterns taken form 304L and Al sheets. The 304L material was basically austenitic with some weak strain-induced martensite [22] peaks. Fig. 4 also shows the XRD patterns taken from the 304L side and Al side of the M_{600} after debonding. As discussed before (Section 3.2), the intermediate layer sat on the 304L side of the M_{600} specimen after debonding and no intermetallic phases were found on the Al side of the M_{600} specimen. This was consistent with the observation of crack along the Al/intermediate layer interface as shown in Fig. 2b.

The XRD pattern of M_{600} showed that intermetallics of Al and Fe such as $Al_{13}Fe_4$ and Al_8SiC_7 were possibly the main phases of the intermediate layer, while some other phases could also be detectable from this XRD pattern. These results were consistent with the elemental analysis determined by the EDS point and line scan techniques. It should be noted that the XRD patterns taken from the 304L side and the Al side of the A_{600} after debonding were identical to those taken from the M_{600} specimen (Fig. 4). Therefore, the presence of the martensitic microstructure did not have any noticeable effect upon the phase formation in the intermediate layer.

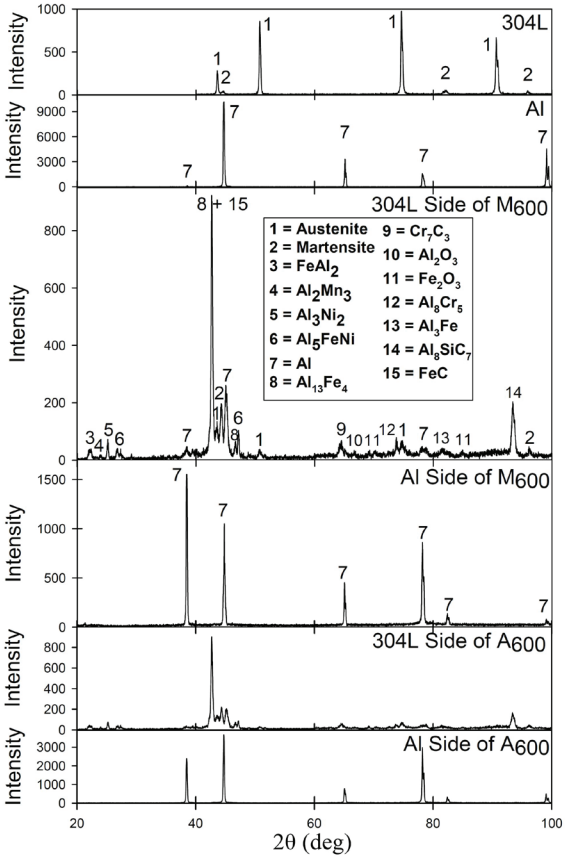

Fig. 4. XRD patterns taken form 304L and Al sheets and 304L side and Al side of the M_{600} and A_{600} after debonding.

3.5. Microhardness measurements

Fig. 5 shows the results of Vickers microhardness measurements taken from several indentations ranging from Al to 304L for both M_{600} and A_{600} specimens. To get reliable microhardness values, the indentations were performed at different points along the rolling direction (RD) with the preservation of correct distances with respect to the interface parallel to the normal direction (ND). It could be easily seen that the hardness values in the intermediate layers were much higher than those of the contacting layers [8, 19].

Moreover, the microhardness values taken from the 304L sheet were considerably higher than those taken from the Al sheet. Furthermore, the hardness values of the 304L sheet were higher for the M_{600} (with an austenitic-martensitic microstructure) than those of the A_{600} (with a completely austenitic microstructure). These findings were consistent with the expected trend [23,24]. However, the difference between the hardness values of the 304L sheets for the M_{600} and A_{600} was not high, which might be connected to the partial reversion of strain-induced martensite to austenite [25,26] after annealing at 600 °C for 1h.

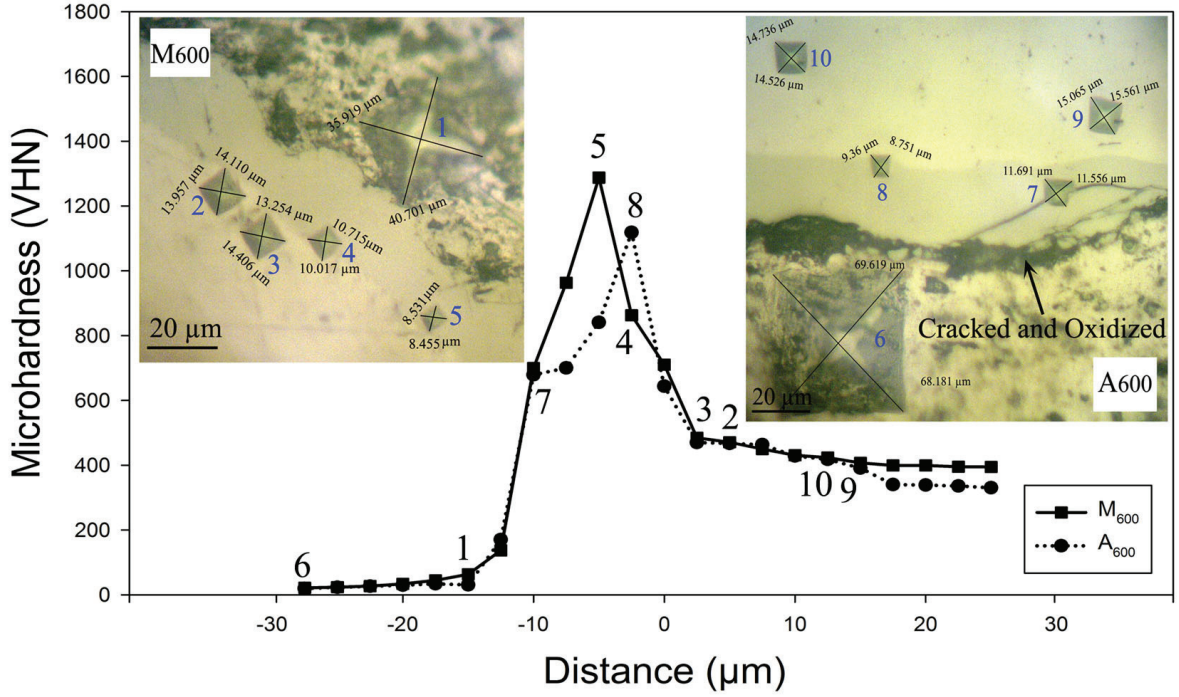

Fig. 5. The results of the Vickers microhardness measurements and the corresponding indentations taken from M600 and A_{600} specimens.

The levels of microhardness values in the intermediate layer were consistent with the microhardness values of the contributing compounds such as $Al_{13}Fe_4$ with the microhardness of 1070 VHN [27] and FeC with the microhardness of 1025 KHN [28], equivalent to 1129 VHN [29].

The hardness values on the 304L sheet near the 304L/intermediate layer interface was somewhat higher than that of the base 304L sheet, which could be related to the diffusion phenomenon. This was also the case for the hardness values on the Al sheet near the Al/intermediate layer interface. The overall hardness profiles taken from the intermediate layers of M_{600} and A_{600} were comparable to each other, which can be ascribed to the completely identical phases with nearly similar peak intensities based on the XRD results shown in Figs. 4.

Based on the microhardness changes, the thickness of the intermediate layer plus the diffused distance could be estimated as ~ 40 µm, which was in a very good agreement with EDS results. Moreover, the thickness of the intermediate layer could be estimated as ~ 17 µm (the distance between indentation numbers 1 and 3), which was consistent with the optical and SEM micrographs (9-17 µm).

4. Discussion

According to Kirkendall effect [15], in a diffusion couple, atoms with a lower melting point possess a higher diffusion coefficient, showing that the diffusion coefficient of Fe in Al is expected to be lower than the diffusion coefficient of Al in Fe. However, it has been found in several studies that the diffusion of Fe in Al is much higher than that of Al in Fe [13, 14, 30-32]. Note that the atomic radius of Fe (0.124 nm) is effectively lower than that of Al (0.143 nm). Therefore, the diffusion of Al in Fe lattice to make substitution Al results in a considerable distortion in the iron lattice. Moreover, since the melting point of Al is ~ 660 °C, it is expected that the diffusion of impurity elements in the Al lattice would be high at 600 °C.

It is generally accepted that the diffusion distance (x) is proportional to $2\sqrt{(Dt)}$ [21]. The results of the calculation of diffusion distances based on the diffusion coefficients determined by various methods are summarized in Table 2. Firstly, this table shows that the diffusion coefficient of Fe in Al was on the order of 5×10^{-14} m^2/s, but the diffusion coefficient of Al in Fe was on the order of 2×10^{-18} m^2/s. Therefore, the diffusivity of Fe in Al was about 4 orders of magnitude larger than that of Al in Fe. It is interesting to note that Fig. 2b also confirms these results, showing that the intermediate layer was formed completely on the Al side of the roll bonded sheet after annealing treatment; this , in turn, reveals that this layer was formed by the diffusion of elements the 304L sheet to the Al sheet. This is also consistent with the results reported for the joining of Al to low-carbon steel by laser roll welding [31]. Secondly, the diffusion distance of Fe in Al was between ~20.84 to 29.5 μm, which was relatively consistent with the diffusion distance determined from the EDS spectra and microhardness profiles.

According to XRD analysis, the intermediate layer was mainly composed of intermetallics of Fe and Al. Contribution of high amount of Al in these compounds (as the host metal) proved this statement. Diffusion of iron into aluminum was much faster than that of aluminum in iron. This condition could be favorable for the formation of Al-rich intermetallic compounds in the interface layer because iron atoms are fewer in number after migrating into the aluminum side [31, 33].

The presence of Si in Al_8SiC_7 intermetallic compound could be due to the high diffusion coefficient

Table 2. Calculations of impurity diffusivity (D) based on Arrhenius equation (T = 873 K and t = 3600 s) and diffusion distance (x) [13, 14, 30].

Guest element	Host element	D_0 (m^2/s)	Q (kJ/mol)	T (K)	Method	D (m^2/s)	x (μm)
Al	Fe	1.8×10^{-4}	228.2	1003-1673	XRD	3.9882×10^{-18}	0.2396
		3.3×10^{-3}	256.1	1048-1183	XRD	1.5653×10^{-18}	0.1502
		2.2×10^{-5}	257	1230-1473	EPMA	9.2185×10^{-21}	0.0116
		5.3×10^{-4}	241.3	1064-1183	EPMA	1.9499×10^{-18}	0.1676
Fe	Al	91	258.7	792–931	IIMLS	3.0169×10^{-14}	20.8430
		1.35×10^{-2}	192.5	823–906	LS	4.0923×10^{-14}	24.2754
		1.1	221.6	892–927	MBS	6.0508×10^{-14}	29.5180
		5.3×10^{-3}	183.4	793–922	MS	5.6288×10^{-14}	28.4702
		7.7×10^{-1}	220.9	723–931	IIMS	4.6644×10^{-14}	25.9166
		4.1×10^{-13}	58.2	632–903	RC	1.3500×10^{-16}	1.3942
		1.2×10^{-5}	134.9	1093–1203	MBS	1.0171×10^{-13}	38.6980
Cr	Al	10	282	873–923	IIMS	1.3377×10^{-16}	1.3878
		5	242.7	859–923	MS	1.5027×10^{-14}	14.7098
		80	255.3	773–918	DCEPMA	4.2369×10^{-14}	24.7004
		6.4	261	690–910	DCEPMA	1.5455×10^{-15}	4.7176
		3×10^{-11}	64.4	523–878	RC	4.2044×10^{-15}	7.7810
Mn	Al	8.7×10^{-3}	208.2	743–929	IIMS	3.0320×10^{-15}	6.6076
		3.8×10^{-2}	221.8	773–918	DCEPMA	2.0335×10^{-15}	5.4112
		2.2×10^{-5}	120.5	729–916	LS	1.3559×10^{-12}	139.7316
		1.3×10^{-1}	228.9	773–923	DCEPMA	2.6155×10^{-15}	6.1370
		10-2	211.4	730–921	IIMS	2.2426×10^{-15}	5.6826
		3.2×10^{-2}	217	843–927	MS	3.3175×10^{-15}	6.9118
Ni	Al	2.9×10^{-12}	65.7	632–902	RA	3.3978×10^{-16}	2.2120
		4.4×10^{-4}	145.8	742–924	RM	8.3064×10^{-13}	109.3674
Si	Al	1.8×10^{-3}	150.6	623–823	DCEPMA	1.7540×10^{-12}	158.9252
		9×10^{-5}	127.8	738–873	DCM	2.0288×10^{-12}	170.9244
		3.5×10^{-5}	123.9	618–904	DCEPMA	1.3503×10^{-12}	139.4428
		2.6×10^{-4}	136.8	754–905	RC	1.6961×10^{-12}	156.2820
		2×10^{-4}	136	753–893	DCEPMA	1.4567×10^{-12}	144.8344
Mo	Al	1.4×10^{-3}	250	898-928	EPMA	1.5389×10^{-18}	0.1488

Table 3. Atomic radiuses of the contributing elements [21].

element	Al	Fe	Ni	Mn	Cr	Mo	Si	C
Atomic radius (nm)	0.143	0.124	0.125	0.112	0.125	0.136	0.118	0.071

of Si in Al, as compared to other elements present in the stainless steel sheet (Table 2). Moreover, the contribution of carbon in some phases could be related to the fast interstitial diffusion mechanism. It should be noted that the absence of Mo in the intermediate layer could be attributed to the low diffusion coefficient (Table 2). All such elements, which were present in the stainless steel, had a smaller atomic radius than aluminum, as shown in Table 3. However, the difference between the atomic radiuses of Al and Mo was not so high. These differences in atomic radiuses and their relation with diffusion coefficients are in accordance with the obtained results.

5. Conclusions

To summarize, the reduction in the thickness of <10% was found to be the threshold reduction for the cold roll bonding process of Al-clad stainless steel sheets. The intermetallics of Al and Fe were found to be the main phases of the intermediate layer after post annealing at 600 °C. It was found that the presence of strain-induced martensite did not exert any noticeable effect on this layer, but increased the hardness of the 304L sheet. Moreover, the calculated diffusion distances were in a good agreement with the results obtained from the line scan EDS analysis and the microhardness profile. It was found that the intermediate layer was formed completely on the Al side of the roll bonded sheet, indicating the faster diffusion of Fe in Al.

References

[1] J.Y. Jin and S.I. Hong: Mater. Sci. Eng. A, 596(2014), 1.
[2] H.G. Kang, J.K. Kim, M.Y. Huh and O. Engler: Mater. Sci. Eng. A., 452-453(2007), 347.
[3] J.E. Lee, D.H. Bae, W.S. Chung, K.H. Kim, J.H. Lee and Y.R. Cho: J. Mater. Process. Technol., 452-453(2007), 546.
[4] I.K. Kim and S.I. Hong: Mater. Des., 49 (2013), 935.
[5] M. Shirdel, H. Mirzadeh, and M.H. Parsa: Mater. Charact., 103(2015), 150.
[6] K.S. Lee, D.H. Yoon, H.K. Kim, Y.N. Kwon and Y.S. Lee: Mater. Sci. Eng. A, 556(2012), 319.
[7] N. Masahashi, K. Komatsu, S. Watanabe and S. Hanada: J. Alloys and Compd., 379(2004), 272.
[8] M. Movahedi, A.H. Kokabi and S.M. Seyed Reihani: Mater. Des., 32(2011), 3143.
[9] X.K. Peng, R. Wuhrer, G. Heness and W.Y. Yeung: J. Mater. Sci., 34(1999), 2029.
[10] C.Y. Chen, H.L. Chen and W.S. Hwang: Mater. Trans., 47(2006), 1232.
[11] H. Danesh Manesh and A. Karimi Taheri: Mater. Des., 24(2003), 617.
[12] Q. Wang, X.S. Leng and T.H. Yang: Trans. Nonferrous Metals Soc. China, 24(2014), 279.
[13] G. Neumann and C. Tuijn: Self-diffusion and Impurity Diffusion in Pure Metals: Handbook of Experimental Data, Elsevier, (2011).
[14] Y. Du, Y.A. Chang, B. Huang, W. Gong, Z. Jin, H. Xu, Z. Yuan, Y. Liu, Y. He and F-Y Xie: Mater. Sci. Eng. A, 363(2003), 140.
[15] D.A. Porter and K.E. Easterling: Phase Transformation in Metals and Alloys, 2nd ed, Chapman & Hall, London, (1992).
[16] M.A Soltani, R. Jamaati and M.R. Toroghinejad: Mater. Sci. Eng. A, 550(2012), 367.
[17] H.R. Akramifard, H. Mirzadeh and M.H. Parsa: Mater. Sci. Eng. A, 613(2014), 232.
[18] H.R. Akramifard, H. Mirzadeh and M.H. Parsa: Mater. Des., 64(2014), 307.
[19] X. Li, G. Zu, M. Ding, Y. Mu and P. Wang: Mater. Sci. Eng. A, 529(2011), 485.
[20] D.R. Askeland, P.P. Fulay and W.J. Wright: The Science and Engineering of Materials, 6th ed, CENGAGE Learning, (2011).
[21] W.D. Callister and D.G. Rethwisch: Materials Science and Engineering, 8th ed, Wiley, (2010).
[22] H. Mirzadeh and A. Najafizadeh: Mater. Charact., 59(2008), 1650.
[23] K.H. Lo, C.H. Shek and J.K.L. Lai: Mater. Sci. Eng. R, 65(2009), 39.
[24] H. Mirzadeh and A. Najafizadeh: J. Alloys Compd., 476(2009), 352.
[25] H. Mirzadeh and A. Najafizadeh: Mater. Des., 30(2009), 570.
[26] M. Naghizadeh and H. Mirzadeh: Metall. Mater. Trans. A., 47(2016), 4210.
[27] J.M. Dubois and E. Belin-Ferre: Complex Metallic Alloys: Fundamentals and Applications, John Wiley & Sons, (2010).
[28] W. Glaeser: Materials for Tribology, Elsevier, (1992).
[29] Hardness conversion of metals, http://www.tribology-abc.com/calculators/hardness.htm, (2014).
[30] S. Kobayashi and T. Yakou: Mater. Sci. Eng. A, 338(2002), 44.
[31] M.J. Rathod and M. Kutsuna: Weld. J., 83(2004), 16.
[32] Y. Li, J. Wang, Y. Yin and H. Ma: Bull. Mater. Sci., 28(2005), 69.
[33] G. Stergioudis: J. Alloys Compd., 403(2005), 143.